Dalton Transactions

Cite this: *Dalton Trans.*, 2012, **41**, 6957

www.rsc.org/dalton

PAPER

A C_2-symmetric antimonato polyoxovanadate cluster $[V_{16}Sb_4O_{42}(H_2O)]^{8-}$ derived from the $\{V_{18}O_{42}\}$ archetype†

Elena Antonova,[a] Christian Näther,[a] Paul Kögerler[b] and Wolfgang Bensch*[a]

Received 13th February 2012, Accepted 21st March 2012
DOI: 10.1039/c2dt30319a

The new antimonato polyoxovanadate $[V^{IV}{}_{16}Sb^{III}{}_4O_{42}(H_2O)]^{8-}$ cluster (**1a**) is the main structural motif of the solvothermally obtained compound $\{(trenH_2)Zn(tren)\}_2[V_{16}Sb_4O_{42}(H_2O)]\cdot xH_2O$ (x = 6–10) (**1**) (tren = tris(2-aminoethyl)amine). The C_2-symmetric cluster structure is closely related to the $\{V_{18}O_{42}\}$ archetype. **1** crystallizes in the monoclinic space group $C2/c$ with a = 30.7070(19) Å, b = 13.9512(5) Å, c = 23.1435(14) Å, β = 128.076(6)°, and V = 7804.8(7) Å^3. The orientation of the $[Sb^{III}{}_2O_5]^{4-}$ groups in each cluster leads to intermolecular Sb···O contacts and the formation of channels between the clusters. $[Zn(tren)(trenH_2)]$ complexes with trigonal bipyramidal coordination environments are located between the $[V_{16}Sb_4O_{42}(H_2O)]^{8-}$ anions, and form a three dimensional network with them *via* strong N–H···O hydrogen bonds. Up to 250 °C crystal water molecules are emitted, which are reversibly incorporated in humid air.

Introduction

The class of polyoxovanadate (POV)-based materials generates increasing interest not only due to a diversity of cluster structures, but also due to their potential use in supramolecular, analytical and clinical chemistry to medicine, as electronic and protic conductors, in batteries and in nanoscale magnetic materials.[1–6] Several reduced POVs (containing V^{IV} spin centers) have been used as model systems to explore unusual magnetic properties,[7,8] several of them linked to geometrical spin frustration.[9]

Importantly, POV clusters have been successfully modified, *e.g.* by substituting VO_5 pyramids of the cluster shells by heteroatoms such as As,[10–21] Sb,[22–28] Ge,[29–32] or Si.[33–35] Compared to the arsenato POVs with typical compositions $[V_{14}As_8O_{42}]^{4-}$, $[V_{15}As_6O_{42}]^{6-}$, or $[V_{16}As_4O_{42}]^{8-}$, analogous antimony-substituted polyoxovanadates are less explored (primarily due to solubility issues of antimony reactants) and therefore their physical properties are barely investigated. Antimony-modified POVs significantly expand the area of POV chemistry due to the introduction of a different functionality compared to the As-containing congeners. Several properties of antimony-based POVs are promising for different potential applications like in sorption,[36] selective oxidation reactions,[37] and as deNOx catalysts[4] or heterogeneous oxidation catalysts.[38] Further investigations have shown that the antimony cations have a stabilizing effect on polyoxometalates at high temperatures.[39]

Recently, we and others were able to synthesize Sb-based POV clusters like $[V_{14}Sb_8O_{42}]^{4-}$, $[V_{15}Sb_6O_{42}]^{6-}$, and $[V_{16}Sb_4O_{42}]^{8-}$ both as discrete architectures as well as 2D or 3D networks.[22–28] Additionally, we successfully modified such anions by covalent attachment of organic molecules to the POV cluster shell, for example in $[V^{IV}{}_{14}Sb^{III}{}_8(aep)_4O_{42}(H_2O)]\cdot 4H_2O$ and $(aepH_2)_2[V^{IV}{}_{15}Sb^{III}{}_6(aep)_2O_{42}(H_2O)]\cdot 2.5H_2O$ (aep = *N*-(2-aminoethyl)piperazine),[40] in two pseudopolymorphic $\{Ni(dien)_2\}_3[V_{15}Sb_6O_{42}(H_2O)]\cdot xH_2O$ (x = 8, 12) and $\{Ni(dien)_2\}_4[V_{16}Sb_4O_{42}(H_2O)]$ (dien = diethylenetriamine).[41]

In this work we present details about the synthesis and characterization of the new compound $\{(trenH_2)Zn(tren)\}_2[V_{16}Sb_4O_{42}(H_2O)]\cdot xH_2O$ (**1**), comprising the spherical cluster shell $[V_{16}Sb_4O_{42}(H_2O)]^{8-}$ (**1a**). In contrast to all hitherto reported analogues, $[V_{16}Sb_4O_{42}(H_2O)]^{8-}$ and $[V_{16}As_4O_{42}(H_2O)]^{8-}$, which exhibit a D_{2h}-symmetric $\{V_{16}\}$ skeleton, the position of $\{Sb_2\}$ groups in **1a** reduced the symmetry of its metal skeleton to C_2.

Results and discussion

Compound **1** crystallizes in the monoclinic space group $C2/c$ with four formula units per unit cell. Selected crystal data and details of the structure determination are summarized in Table 1.

The main structural motif in the crystal lattice of **1** is the $[V_{16}Sb_4O_{42}(H_2O)]^{8-}$ cluster with one H_2O guest encapsulated at the center of the spherical shell (Fig. 1). The distances between its oxygen atom and the V centers of the cluster range from 3.7095(1) to 3.9538(1) Å. The spherical shell is derived from the

[a]*Christian-Albrechts-Universität zu Kiel, Institut für Anorganische Chemie, D-24098 Kiel, Germany. E-mail: wbensch@ac.uni-kiel.de; Fax: +49 431 880 1520; Tel: +49 431 880 2091*
[b]*RWTH Aachen University, Institut für Anorganische Chemie, D-52074 Aachen, Germany*

†Electronic supplementary information (ESI) available. CCDC 866641. For ESI and crystallographic data in CIF or other electronic format see DOI: 10.1039/c2dt30319a

$\{V_{18}O_{42}\}$ archetype by substituting two VO_5 pyramids by two Sb_2O_5 handles being composed of corner-linked SbO_3 groups (Sb–O bond lengths: 1.947(4)–1.966(4) Å; Sb–O–Sb bond angle: 93.74(17)–98.22(17)°) (Tables S1 and S2, ESI†), resulting in a total of 16 VO_5 square pyramids and 2 Sb_2O_5 moieties.

Eight edge-sharing VO_5 pyramids form the central ring being capped by four edge-sharing VO_5 polyhedra on each side. The caps are perpendicular to the ring but not to each other and share edges with the VO_5 pyramids of the central ring.

Bond valence sum (BVS) calculations show that the oxidation state of all V centers is close to +4 (3.96–4.13, see Table S3†), which is consistent with the charge balance and is also confirmed by the strong, unsplit band at 954 cm^{-1} in the IR spectrum. BVS calculations for the Sb atoms yield the values 3.11 and 3.21 for Sb1 and Sb2, respectively, and for Zn^{2+} yield 2.27.

In contrast to other cluster anions $[V_{16}Pn_4O_{42}(H_2O)]^{8-}$ (*Pn* = As, Sb) that comprise D_{2h}-symmetric $\{V_{16}\}$ skeletons,[42] the $\{V_{16}\}$ substructure in **1a** in stark contrast exhibits C_2 symmetry (Fig. 1 and 2). The resulting pseudorhombicuboctahedron formed by the 20 μ_3-bridging oxygen atoms can formally be derived from the rhombicuboctahedron by 45° rotation of one half (Fig. 2).

Like in all polyoxovanadate clusters based on the $\{V_{18}O_{42}\}$ archetype, long basal V–O (1.910(4)–2.022(4) Å) and shorter terminal V=O (1.607(4)–1.645(4) Å) bonds are observed (Table 2).

The shortest V–V distances are between 2.729(2) and 3.1013 (13) Å (avg. 2.915 Å; Δ 0.3723 Å). A detailed comparison with the geometric parameters of other $[V_{16}Pn_4O_{42}(H_2O)]^{8-}$ clusters with D_{2h} symmetry reveals some significant differences, especially for the V···V distances. In the $[V_{16}Sb_4O_{42}(H_2O)]^{8-}$ shells the V···V separations vary from 2.8451(17) to 3.0607(17) (avg. 2.98; Δ 0.2156 Å) for $[C_6H_{17}N_3]_4[Sb_4V_{16}O_{42}]\cdot 2H_2O$,[24] from 2.9067(9) to 3.0341(9) (avg. 2.96; Δ 0.1274 Å) for $[V_{16}Sb_4O_{42}(H_2O)\{VO(C_6H_{14}N_2)_2\}_4]\cdot 10H_2O\cdot C_6H_{14}N_2$,[26] and from 2.9145(8) to 3.0468(8) (avg. 2.96;Δ 0.1323 Å) for $[Zn_2(dien)_3][\{Zn(dien)\}_2V_{16}Sb_4O_{42}(H_2O)]\cdot 4H_2O$.[28] Similar values are also found for the $[V_{16}As_4O_{42}(H_2O)]^{8-}$ cluster (2.9105(12)–3.0427(11) Å; avg. 2.98 Å; Δ 0.1322 Å).[42]

There are one crystallographically independent Zn^{2+} cation and two tren groups located on general positions. The Zn^{2+} ion coordinates to four N atoms from one tetradentate neutral tren ligand and one N donor from the second (doubly protonated) $trenH_2$ (Fig. 3). This binding mode of tren has been observed in $[Co(tren)(trenH_2)]_2\{[Co(tren)]_2V_{15}Ge_6O_{42}S_6(H_2O)\}\cdot 9H_2O$[43]

Table 1 Selected crystal data and details of the structure determination of **1**

Sum formula	$C_{24}H_{90}N_{16}O_{49}Sb_4V_{16}Zn_2$
Formula weight	2819.8804
Crystal system	Monoclinic
Space group	*C*2/*c*
a/Å	30.7070(19)
b/Å	13.9512(5)
c/Å	23.1435(14)
β	128.076(6)°
V/Å^3	7804.8(7)
Z	4
Density/g cm^{-3}	2.384
Reflections collected	36 771
Independent reflections	9130
R_{int}	0.0698
R_1 for $[I > 2\sigma(I)]$	0.0427
GooF	1.005
wR_2 for all reflections	0.0952
T/K	293

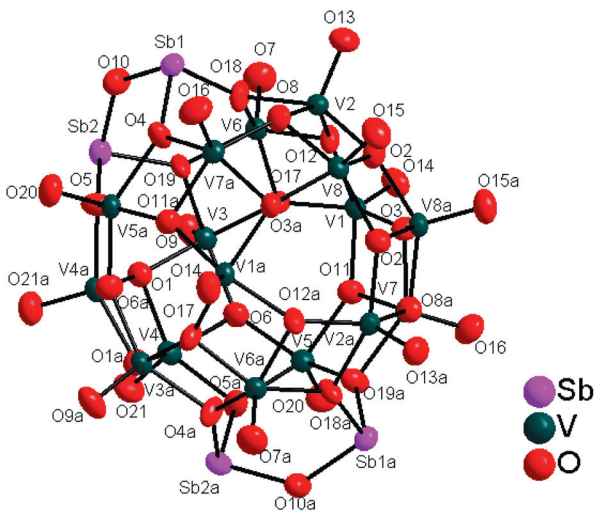

Fig. 1 The $[V_{16}Sb^{I}_4O_{42}(H_2O)]^{8-}$ anion of compound **1** using displacement ellipsoids (50% probability level). The water molecule at the centre of the cluster is not shown for clarity.

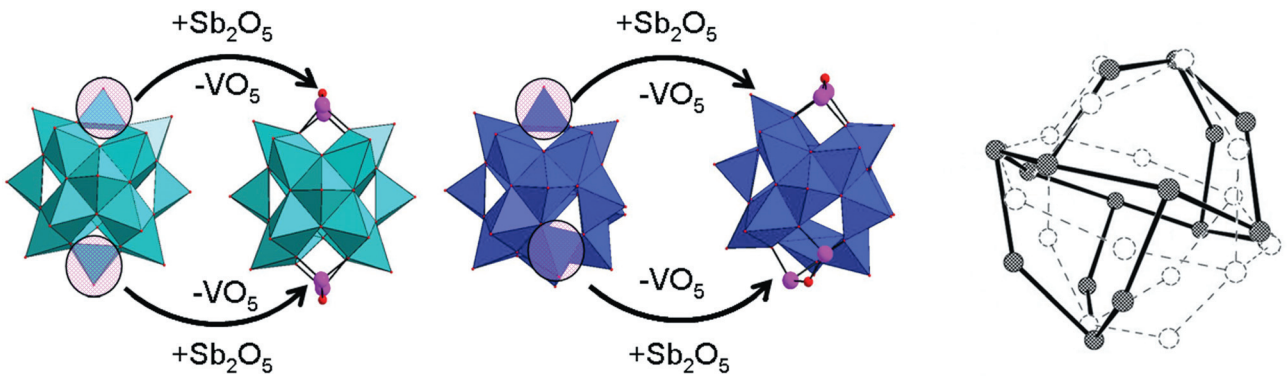

Fig. 2 Left: the previously reported $[V_{16}Sb_4O_{42}]^{8-}$ cluster with D_{2h}-symmetry. Middle: the $[V_{16}Sb_4O_{42}]^{8-}$ cluster **1a**. Right: overlay of the $\{V_{16}\}$ skeletons of the two $[V_{16}Sb_4O_{42}]^{8-}$ cluster types; dashed: D_{2h}-symmetric $\{V_{16}\}$; solid: C_2-symmetric $\{V_{16}\}$.

Table 2 V–O bond lengths of compound **1**. Estimated standard deviations are given in parentheses

V–O	Å	V–O	Å	V–O	Å	V–O	Å
V(1)–O(14)	1.638(4)	V(3)–O(9)	1.607(4)	V(5)–O(20)	1.607(4)	V(7)–O(16)	1.641(4)
V(1)–O(17)	1.922(4)	V(3)–O(17)	1.910(4)	V(5)–O(6)	1.939(4)	V(7)–O(3)	1.923(4)
V(1)–O(3)	1.940(4)	V(3)–O(6)	1.932(4)	V(5)–O(11)	1.959(4)	V(7)–O(11)	1.926(4)
V(1)–O(11)	1.957(4)	V(3)–O(1)	1.978(4)	V(5)–O(19)#1[a]	2.012(4)	V(7)–O(8)#1[a]	1.963(4)
V(1)–O(12)	1.971(4)	V(3)–O(4)	2.005(4)	V(5)–O(5)#1[a]	2.022(4)	V(7)–O(19)#1[a]	2.016(4)
V(2)–O(13)	1.624(4)	V(4)–O(6)	1.925(4)	V(6)–O(7)	1.631(4)	V(8)–O(15)	1.645(4)
V(2)–O(12)	1.931(4)	V(4)–O(1)	1.946(4)	V(6)–O(17)	1.920(4)	V(8)–O(3)#1[a]	1.920(4)
V(2)–O(2)	1.940(4)	V(4)–O(5)#1[a]	2.020(4)	V(6)–O(12)	1.943(4)	V(8)–O(2)	1.941(4)
V(2)–O(8)	1.962(4)	V(4)–O(21)	1.636(4)	V(6)–O(4)	1.963(4)	V(8)–O(2)#1[a]	1.941(4)
V(2)–O(18)	2.007(4)	V(4)–O(1)#1[a]	1.921(4)	V(6)–O(18)	1.970(4)	V(8)–O(8)	1.989(4)

[a] Atoms marked with #1 generated by symmetry transformation $-x, y, -z + 1/2$.

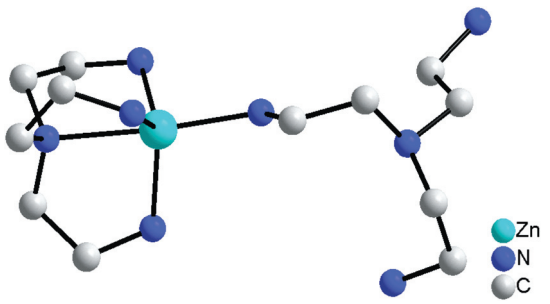

Fig. 3 The transition metal complex $[(N_4C_6H_{20})Zn(N_4C_6H_{18})]^{4+}$.

with a doubly protonated trenH$_2$ group as in compound **1**, and in [Mn(tren)(trenH)]SbS$_4$ with a monoprotonated amine.[44] This binding mode of tren was also found in the structures of [Mn(tren)$_2$]Cl$_2$,[45] Mn$_2$(tren)$_3$[Mo$_2$O$_2$S$_6$]$_2$·3H$_2$O,[46] [Ni$_3$(tren)$_4$(H$_2$O)$_2$][Cr(oxalate)$_3$]$_2$·6H$_2$O,[47] Ni$_2$(tren)$_3$(Mo$_2$O$_2$S$_6$)$_2$·2.75H$_2$O,[48] Co$_2$(tren)$_3$(MoS$_4$)$_2$,[48] and [Cd$_7$(tren)$_{12}$](ClO$_4$)$_{14}$ [49] all containing neutral tren. The resulting ZnN$_5$ trigonal bipyramid is severely distorted with Zn–N bonds from 2.066(6) to 2.269(5) Å (Table S4†). The Zn–N bond lengths are in agreement with published data.[50–53]

In **1**, the clusters are arranged in layers parallel to the (010) plane. The water molecules and the Zn^{2+} complexes occupy the area between these layers. Along the *a*- and *c*-axes the layers alternate in an ...ABAB... fashion (Fig. S1†) and the cluster anions are arranged so that the Sb$_2$O$_5$ units alternate up and down. The Zn(tren)$_2$ moieties of the $[(trenH_2)Zn(tren)]^{4+}$ complexes are directed towards each other forming pairs (Fig. S2†).

In total, 15 N–H···O hydrogen bonds (2.775–3.471 Å) are identified between the Zn^{2+} complexes and the clusters anion and/or water molecules (Table 3, Fig. 4). This interlinks three cluster anions and one complex cation to a 2D network. The weaker Sb···O interactions expand this into a 3D network.

Thermogravimetric analysis shows that **1** decomposes with a total mass loss of Δ_{mexp} = 49.5 wt% in the temperature range from 30 to 800 °C, accompanied by endothermic events. The first mass loss covers a large temperature range from 30 to 250 °C (Δ_{mexp} = 4.3 wt%), and is due to the loss of 7 water molecules as confirmed by mass spectrometry (Fig. 5).

The simultaneous emission of a tren fragment and water molecules occurs at *ca.* 358 °C and is accompanied by an intense

Table 3 Hydrogen bond lengths (Å) and angles (°). Estimated standard deviations are given in parentheses

D–H	*d*(H..A)	∠DHA	*d*(D..A)	A
N8–H8A	1.92	161.30	2.774 (7)	O14
N8–H8B	1.96	162.5	2.817(7)	O16#1[a]
N8–H8C	2.17	167.8	3.044(9)	O23
N3–H3A	1.95	162.0	2.817(7)	O21#2[a]
N3–H3B	2.30	154.2	3.137(11)	O24#3[a]
N2–H2A	2.05	158.1	2.906(7)	O9#1[a]
N2–H2B	2.28	149.5	3.087(7)	O20#2[a]
N5–H5A	2.15	170.6	3.039(7)	O14#1[a]
N5–H5B	2.38	156.0	3.221(7)	O15#3[a]
N1–H1C	2.64	154.6	3.471(7)	O16
N1–H1D	2.09	145.1	2.878(8)	O7#1[a]
N7–H7C	2.11	165.4	2.977(8)	O15
N7–H7D	2.44	148.1	3.235(8)	O21#2[a]
N7–H7D	2.54	111.9	2.991(8)	O21#4[a]
N7–H7E	2.29	137.9	3.012(8)	O15#3[a]

[a] Atoms marked with # generated by symmetry transformations (#1: $-x, -y + 1, -z + 1$; #2: $x, y + 1, z$; #3: $-x, y, -z + 1/2$; #4: $-x, y + 1, -z + 1/2$).

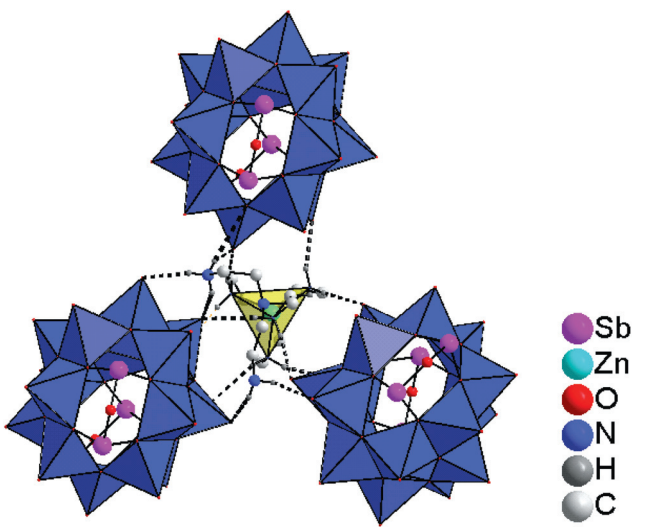

Fig. 4 Three clusters connected to a transition metal complex by hydrogen bonds. Aliphatic H atoms are omitted.

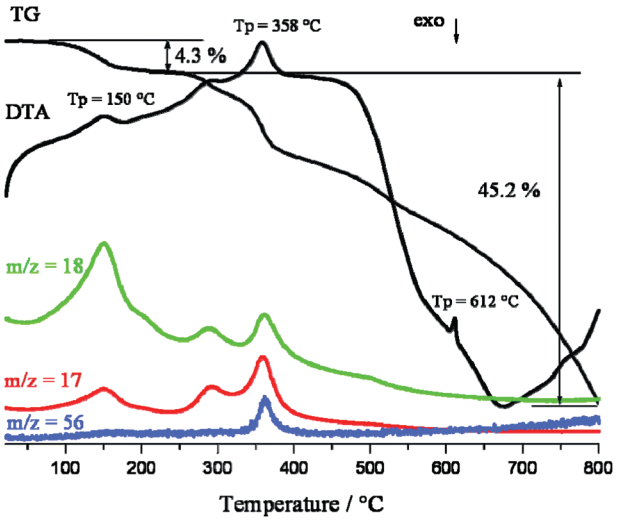

Fig. 5 DTA-TG-MS trend scan curves of 1. Intensities of the signals are in standardized units, *m/z* 17 = OH; *m/z* 18 = H_2O and *m/z* 56 = $C_2N_2H_4$ – fragment of the tren molecule. Gas flow 75 mL min^{-1}.

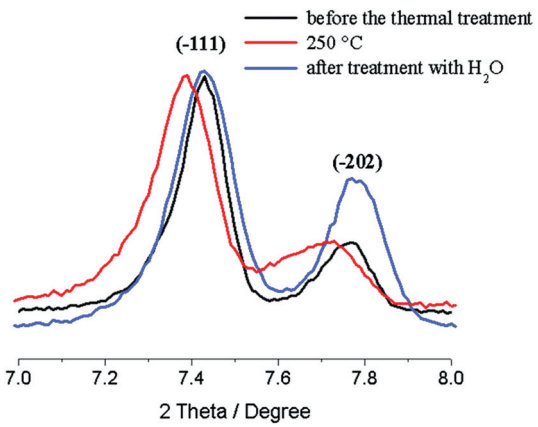

Fig. 6 X-ray powder patterns of 1 in the range of 7–8° 2θ after different treatments. Measured before the thermal treatment: black line; measured after the thermal treatment (250 °C): red line/green line; measured after treatment with H_2O: blue line.

endothermic peak. The decomposition reaction is not complete at 800 °C and the decomposition product at 800 °C was identified as V_2O_3 and SbZn. The endothermic event at 612 °C is due to melting of the vanadium oxide.

To examine whether the compound remains intact after loss of water, a sample was heated to 250 °C and the product was investigated by X-ray powder diffraction. In the powder pattern intense reflections can be observed between 2θ = 7 and 8° (Fig. 6). The reflections exhibit a shift to smaller 2θ values compared to those of the genuine material. Such behavior was already observed for $(Ni(N_3C_5H_{15})_2)_2[\{Ni(N_3C_5H_{15})_2\}V_{15}Sb_6O_{42}(H_2O)]\cdot 8H_2O$ ($N_3C_5H_{15}$ = *N*-(2-aminoethyl)-1,3-propanediamine).[54] The CHN analysis of the sample heated to 250 °C exhibits only a minute loss of organic components (CHN before: C 9.94, H 3.4, N 7.5%; CHN after thermal treatment: 9.29, 2.9, 7.42%). After storing the sample in water overnight at room temperature, both reflections shifted back to the original position (Fig. 6).

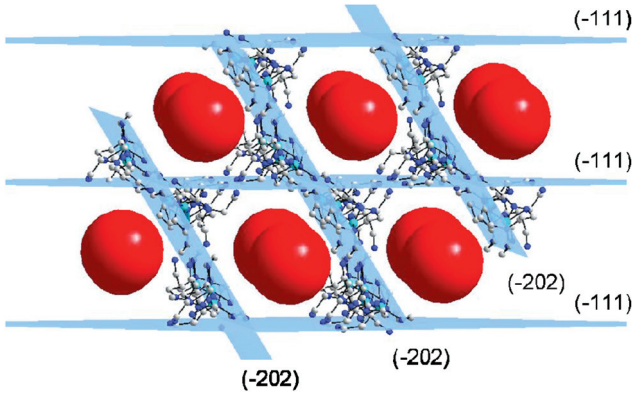

Fig. 7 Arrangement of the clusters in compound **1**. The (−111) and (−202) planes are highlighted in light blue. The clusters are illustrated as red balls.

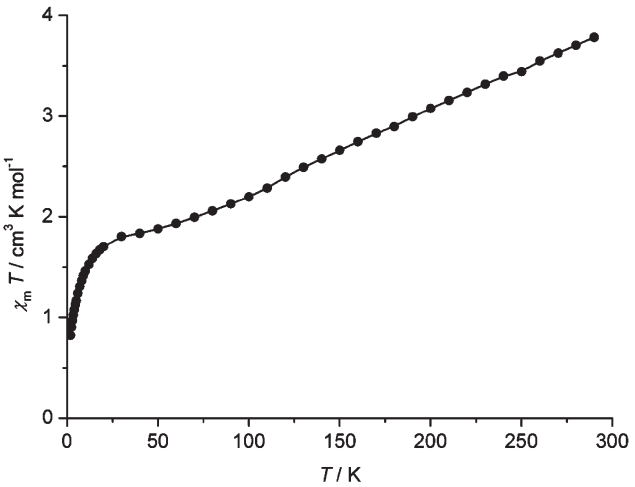

Fig. 8 Temperature dependence of $\chi_m T$ for **1** at 0.1 Tesla. The solid graph represents a visualization aid.

The (−111) and (−202) layers host the water molecules and transition metal complexes (Fig. 7). The shift of both peaks to lower 2θ values upon heating indicates a decrease of the distance between the clusters. Unfortunately, the quality of the single crystals after the thermal treatment was too low for single crystal structure analysis.

UV spectra demonstrate that the compound is soluble in ethanol and methanol (Fig. S3†). The absorption maxima of the UV spectra occur at 225 nm for ethanol and at 220 nm for methanol solutions.

The low-field magnetic susceptibility of **1** indicates strong antiferromagnetic coupling between the spin-1/2 vanadyl groups that is typical for polyoxovanadate(IV) shell-type cluster anions. Consequently, $\chi_m T$ increases only to 3.8 cm^3 K mol^{-1}, well below the value of 6.0 cm^3 K mol^{-1} for 16 uncoupled vanadyl groups (for g_{iso} = 2.0). Between 20 and 70 K the $\chi_m T$ *vs.* *T* graph displays a well-defined broad shoulder at approx. 1.8 cm^3 K mol^{-1}, formally comparable to the value expected for five uncoupled *s* = 1/2 spin centers (Fig. 8). Towards lower temperatures, $\chi_m T$ drops sharply, and a singlet ground state appears

plausible for **1a**. Note that the observed susceptibility data for this C_2-symmetric V_{16} spin polytope drastically differ from the reported data for $[Zn_2(dien)_3]\{[Zn(dien)]_2V_{16}As_4O_{42}(H_2O)\}\cdot 3H_2O$ comprising a D_{2h}-symmetric V_{16} polytope,[42] where no plateau or shoulder is observed and much stronger AF coupling results in a continuous increase of $\chi_m T$ with increasing temperature to reach a room temperature value of only approx. 2.4 cm^3 K mol^{-1}. This highlights the essential role of connectivity modes of the $V(=O)O_4$ pyramids in $\{V^{IV}{}_{18}O_{42}\}$-derived spin structures for the resulting magnetism. However, we note that the multitude of exchange pathways in **1a**, including –O–, –O–Sb^{III}–O–, and weaker –O–Sb^{III}–O–Sb^{III}–O– bridges, results in numerous distinct exchange energies and, due to over-parametrization, effectively prevents fitting the available susceptibility data to *e.g.* a simple Heisenberg exchange-type spin Hamiltonian; additional low-temperature magnetization, ESR, and inelastic neutron scattering data will be required to unambiguously establish a model formulation.[55]

Conclusions

All $[V_{16}Pn_4O_{42}(H_2O)]^{8-}$ (*Pn* = As, Sb) cluster shells reported in the past exhibited a D_{2h}-symmetric $\{V_{16}\}$ skeleton. The title compound represents the first example for such a cluster shell with a different symmetry of the $\{V_{16}\}$ skeleton. The symmetry reduction is caused by the different positions of the Sb_2O_5 moieties in the $[V_{16}Sb_4O_{42}(H_2O)]^{8-}$ cluster. While geometric parameters like V–O and Sb–O bond lengths are only slightly affected by the symmetry change, the V–V separations are different to those of other $[V_{16}Pn_4O_{42}(H_2O)]^{8-}$ ions and they scatter over a larger range compared to clusters with approximate D_{2h}-symmetry. Hence the magnetic properties of the title compound are totally different due to altered exchange pathways between the V^{IV} d^1 centers. The UV-spectra of methanol and ethanol solutions evidence that the cluster is soluble in these solvents. The compound is stable up to 250 °C, as confirmed by X-ray powder patterns.

Experimental

Syntheses of the compound

A mixture of 1.1 mmol NH_4VO_3, 0.4 mmol Sb_2O_3 and 0.4 mmol $Zn(NO_3)_2\cdot 6H_2O$ in 4 mL of a 50% aqueous tren solution was sealed in a 30 mL PTFE-lined stainless steel autoclave and heated to 130 °C for 7 days. The pH of the reaction mixture before the synthesis was 12.5 and decreased to 12.2 in the course of the reaction. After cooling to room temperature the precipitate was filtered and washed with water and acetone, and dried in vacuum. Compound **1** consists of brown agglomerates consisting of small rectangular crystallites (Fig. 9). Yield: 47% based on Sb. Elemental analysis: C 9.94, H 3.4, N 7.5%, calcd C 10.2, H 3.2, N 7.9%. IR (ν/cm^{-1}): 3224 (m), 3142 (m), 2938 (w), 2872 (w), 1576 (m), 1472 (m), 1363 (w), 1320 (w), 1284, 1130 (w), 1078 (m), 954 (s), 712 (s), 679 (m), 625 (m), 534 (m), 451 (m), 389 (m).

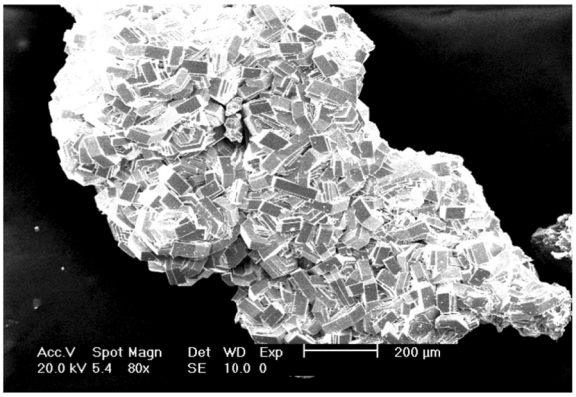

Fig. 9 SEM micrograph of crystals of **1**.

Crystal structure determination

The X-ray intensity data of a single crystal of compound **1** with dimensions of 0.080 × 0.091 × 0.106 mm^3 were collected at room temperature using a STOE-1 Imaging Plate Diffraction System (IPDS-1) with Mo Kα radiation (λ = 0.71073 Å). The raw intensities were treated by standard procedure applying Lorentz polarization as well as absorption correction. Selected crystal data and details of the structure determination are summarized in Table 1. The structure was solved by direct methods with SHELXS-97.[56] Crystal structure refinements were done against F^2 using SHELXL-97.[56] The CH and NH hydrogen atoms were positioned with idealized geometry and refined using a riding model. The H atoms from water were not located. A numerical absorption correction was performed (T_{min}/T_{max} 0.5302, 0.5729). Crystallographic data have been deposited in the Cambridge Crystallographic Data Centre as supplementary publication no. CCDC 866641.

Elemental analysis

CHN analyses were done using a EURO EA Elemental Analyzer, fabricated by EURO VECTOR Instruments and Software.

IR spectroscopy

IR/NIR spectroscopy investigations were performed at room temperature using an Alpha P FT-IR spectrometer from Bruker. The IR spectra were measured from 400 to 4000 cm^{-1}.

Thermal analysis

The DTA-TG investigations were carried out in a nitrogen atmosphere (purity: 5.0; heating rate: 4 K min^{-1}; flow rate: 75 mL min^{-1}; Al_2O_3 crucibles) using a Netzsch STA-409CD instrument, which was equipped with a Balzers QMA 400 Quadrupole Mass Spectrometer.

X-ray powder patterns

X-ray powder patterns were performed on a STOE STADI P diffractometer with a Ge monochromator in transmission mode (Cu Kα radiation, flat sample holders) operated at 40 kV and 30 mA.

Magnetic measurement

Magnetic susceptibility data of **1** were measured in the temperature interval 2.0–290 K at a static external field of 0.1 Tesla using a Quantum Design MPMS-5XL SQUID magnetometer. Data were corrected for the contribution of the sample holder (cylindrical PTFE capsule) and the diamagnetism of compound **1**.

Notes and references

1 M. T. Pope and A. Müller, *Angew. Chem.*, 1991, **103**, 56.
2 M. S. Wittingham, R. Chen, T. Chirayil and P. Y. Zavalij, *Proc. Electrochem. Soc.*, 1996, **76**, 95.
3 J. D. Pless, D. Ko, R. R. Hammond, B. B. Bardin, P. C. Stair and K. R. Poeppelmeier, *J. Catal.*, 2004, **223**, 419.
4 M. I. Khan, S. Tabussum, C. L. Marshall and M. K. Neylon, *Catal. Lett.*, 2006, **112**, 1.
5 A. Müller, H. Reuter and S. Dillinger, *Angew. Chem., Int. Ed. Engl.*, 1995, **34**, 2328; A. Müller, P. Kögerler and C. Kuhlmann, *Chem. Commun.*, 1999, 1347.
6 S. Bertaina, S. Gambarelli, T. Mitra, B. Tsukerblat, A. Müller and B. Barbara, *Nature*, 2008, **453**, 203.
7 I. Chiorescu, W. Wernsdorfer, A. Müller, S. Miyashita and B. Barbara, *Phys. Rev. B: Condens. Matter*, 2003, **67**, 020402.
8 D. Procissi, A. Lascialfari, E. Micotti, M. Bertassi, P. Carretta, Y. Furukawa and P. Kögerler, *Phys. Rev. B: Condens. Matter Mater. Phys.*, 2006, **73**, 184417; A.-L. Barra, L. Pardi, A. Müller and J. Döring, *J. Am. Chem. Soc.*, 1992, **114**, 8509; D. Zipse, N. S. Dalal, R. Vasic, J. S. Brooks and P. Kögerler, *Phys. Rev. B: Condens. Matter Mater. Phys.*, 2005, **71**, 064417; I. Chiorescu, W. Wernsdorfer, A. Müller, H. Bögge and B. Barbara, *Phys. Rev. Lett.*, 2000, **84**, 3454; B. Tsukerblat, A. Tarantul and A. Müller, *J. Chem. Phys.*, 2006, **125**, 054714; Y. Furukawa, Y. Nishisaka, K. Kumagai and P. Kögerler, *J. Magn. Magn. Mater.*, 2007, **310**, 1429; K. Kajiyoshi, T. Kambe, M. Mino, H. Nojiri, P. Kögerler and M. Luban, *J. Magn. Magn. Mater.*, 2007, **310**, 1203.
9 G. Chaboussant, S. T. Ochsenbein, A. Sieber, H.-U. Güdel, H. Mutka, A. Müller and B. Barbara, *Europhys. Lett.*, 2004, **66**, 423.
10 G. Zhou, C. Guo, W. Liu, Y. Xu and X. Zheng, *J. Coord. Chem.*, 2008, **61**, 202.
11 B.-X. Dong, J. Peng, C. J. Gómez-García, S. Benmansour, H.-Q. Jia and N.-H. Hu, *Inorg. Chem.*, 2007, **46**, 5933.
12 Y. Qi, Y. Li, C. Qin, E. Wang, H. Jin, D. Xiao, X. Wang and S. Chang, *Inorg. Chem.*, 2007, **46**, 3217.
13 S.-T. Zheng, Y.-M. Chen, J. Zhang, J.-Q. Xu and G.-Y. Yang, *Eur. J. Inorg. Chem.*, 2006, 397.
14 S.-T. Zheng, J. Zhang and G.-Y. Yang, *J. Mol. Struct.*, 2005, **752**, 25.
15 S.-T. Zheng, M.-H. Wang and G.-Y. Yang, *Inorg. Chem.*, 2007, **46**, 9503.
16 C.-M. Wang, Q.-X. Zeng, J. Zhang and G.-Y. Yang, *J. Cluster Sci.*, 2005, **16**, 65.
17 S.-T. Zheng, J.-Q. Xu and G.-Y. Yang, *J. Cluster Sci.*, 2005, **16**, 23.
18 Y. Qi, Y. Li, E. Wang, H. Jin, Z. Zhang, X. Wang and S. Chang, *J. Solid State Chem.*, 2007, **180**, 382.
19 C. Wang, G. Zhou, Z. Zhang, D. Zhu and Y. Xu, *J. Coord. Chem.*, 2011, **64**, 1198.
20 S.-Y. Shi, Y. Chen, J.-N. Xu, Y.-C. Zou, X.-B. Cui, Y. Wang, T.-G. Wang, J.-Q. Xu and Z.-M. Gao, *CrystEngComm*, 2010, **12**, 1949.
21 Y.-F. Qi, Y.-G. Li, E. Wang, D.-R. Xiao and J. Hua, *J. Coord. Chem.*, 2007, **60**, 1403.
22 L. Zhang, X. Zhao, P. Xu and T. Wang, *J. Chem. Soc., Dalton Trans.*, 2002, 3275.
23 X.-X. Hu, J.-Q. Xu, X.-B. Cui, J.-F. Song and T.-G. Wang, *Inorg. Chem. Commun.*, 2004, **7**, 264.
24 R. Kiebach, C. Näther and W. Bensch, *Solid State Sci.*, 2006, **8**, 964.
25 R. Kiebach, C. Näther, P. Kögerler and W. Bensch, *Dalton Trans.*, 2007, 3221.
26 A. Wutkowski, C. Näther, P. Kögerler and W. Bensch, *Inorg. Chem.*, 2008, **47**, 1916.
27 L. Yu, J.-P. Liu, J.-P. Wang and J.-Y. Niu, *Chem. Res. Chin. Univ.*, 2009, **25**, 426.
28 Y. Gao, Z. Han, Y. Xu and C. Hu, *J. Cluster Sci.*, 2010, **21**, 163.
29 J. Zhou, J. Zhang, W. H. Fang and G. Y. Yang, *Chem.–Eur. J.*, 2010, **16**, 13253.
30 T. Whitfield, X. Wang and A. J. Jacobson, *Inorg. Chem.*, 2003, **42**, 3728.
31 J. Wang, C. Näther, P. Kögerler and W. Bensch, *Inorg. Chim. Acta*, 2010, **363**, 4399.
32 D. Pitzschke, J. Wang, R.-D. Hoffmann, R. Pöttgen and W. Bensch, *Angew. Chem.*, 2006, **118**, 1327.
33 X. Q. Wang, L. M. Liu, G. Zhang and A. J. Jacobson, *Chem. Commun.*, 2001, 2472.
34 A. Tripathi, T. Hughbanks and A. Clearfield, *J. Am. Chem. Soc.*, 2003, **125**, 10528.
35 Y. Gao, Y. Xu, S. Li, Z. Han, Y. Cao, F. Cui and C. Hu, *J. Coord. Chem.*, 2010, **63**, 3373.
36 J. Do and A. J. Jacobson, *Inorg. Chem.*, 2001, **40**, 2468.
37 J. Spengler, F. Anderle, E. Bosch, R. K. Grasselli, B. Pillep, P. Behrens, O. P. Lapina, A. A. Shubin, H.-J. Eberle and H. Knözinger, *J. Phys. Chem. B*, 2001, **105**, 10772.
38 S. Albonetti, F. Cavani, F. Trifiro, M. Gazzano, F. C. Aissi, A. Aboukais and M. J. Guelton, *J. Catal.*, 1994, **146**, 491.
39 F. Cavani, A. Tanguy, F. Trifiro and M. Koutrev, *J. Catal.*, 1998, **174**, 231.
40 E. Antonova, C. Näther, P. Kögerler and W. Bensch, *Angew. Chem.*, 2011, **123**, 790.
41 E. Antonova, C. Näther and W. Bensch, *Dalton Trans.*, 2012, **41**, 1338.
42 S.-T. Zheng, J. Zhang, B. Li and G.-Y. Yang, *Dalton Trans.*, 2008, 5584.
43 J. Wang, C. Näther, P. Kögerler and W. Bensch, *Eur. J. Inorg. Chem.*, 2012, 1237.
44 M. Schaefer, L. Engelke and W. Bensch, *Z. Anorg. Allg. Chem.*, 2003, **629**, 1912.
45 A. Kromm and W. S. Sheldrick, *Z. Anorg. Allg. Chem.*, 2007, **633**, 529.
46 J. Ellermeier and W. Bensch, *Transition Met. Chem.*, 2002, **27**, 763.
47 V. M. Masters, P. V. Bernhardt, L. R. Gahan, B. Moubaraki, K. S. Murray and K. J. Berry, *J. Chem. Soc., Dalton Trans.*, 1999, 2323.
48 J. Ellermeier and W. Bensch, *Z. Naturforsch, B: Chem. Sci.*, 2001, **56**, 611.
49 P. Klüfers and P. Mayer, *Acta Crystallogr., Sect. C: Cryst. Struct. Commun.*, 1998, **54**, 722.
50 S.-T. Zheng, J. Zhang and G.-Y. Yang, *J. Mol. Struct.*, 2005, **752**, 25.
51 S.-T. Zheng, Y.-M. Chen, J. Zhang and G.-Y. Yang, *Z. Anorg. Allg. Chem.*, 2006, **632**, 155.
52 M. Schaefer, R. Stähler, W.-R. Kiebach, C. Näther and W. Bensch, *Z. Anorg. Allg. Chem.*, 2004, **630**, 1816.
53 M. Schaefer, C. Näther and W. Bensch, *Monatsh. Chem.*, 2004, **135**, 461.
54 E. Antonova, C. Näther and W. Bensch, *Inorg. Chem.*, 2012, **51**, 2311.
55 P. Kögerler, B. Tsukerblat and A. Müller, *Dalton Trans.*, 2010, **39**, 21.
56 G. M. Sheldrick, *Acta Crystallogr., Sect. A: Found. Crystallogr.*, 2007, **64**, 112.

